Journal of Materials Science: Materials in Electronics (2018) 29:11901–11909
https://doi.org/10.1007/s10854-018-9291-x

Structure and microwave dielectric properties of $Zn_{0.9}Mg_{0.1}TiO_3$–$Zn_{0.15}Nb_{0.3}Ti_{0.55}O_2$ ceramics with ZnO–B_2O_3–SiO_2 glass

Enzhu Li[1,2] · Yingfeng Yang[1,2] · Hongyu Yang[1,2] · Ying Yuan[1,2] · Shuren Zhang[1,2]

Received: 27 March 2018 / Accepted: 11 May 2018 / Published online: 22 May 2018

Abstract
$(1-x)Zn_{0.9}Mg_{0.1}TiO_3$–$xZn_{0.15}Nb_{0.3}Ti_{0.55}O_2$ ((1 − x)ZMT–xZNT) (x = 0.100, 0.125, 0.150, 0.175, 0.200) ceramics were prepared at 900 °C by conventional mixed-oxide method. The phase content, microstructure and microwave dielectric properties had been investigated in detail. Rietveld refinement shows the coexistence of $Zn_{0.9}Mg_{0.1}TiO_3$, $Zn_{0.15}Nb_{0.3}Ti_{0.55}O_2$, $Zn(BO_2)_2$ and Zn_2TiO_4 phases. With ZnO–B_2O_3–SiO_2 (ZBS) glass added, the ceramics can be sintered well at 900 °C with a smaller grain size of 0.12 μm and a higher relative density (> 95%). The microwave dielectric properties are largely influenced by the phase composition according to mixture rule. A typical sample of 0.825ZMT–0.175ZNT ceramic with optimal dielectric properties (ε_r = 26.14, $Q\times f$ = 27184 GHz, τ_f = − 3.46 ppm °C^{-1}) was sintered at 900 °C for 4 h.

1 Introduction

With the continuing expansion of the microwave communication industry, the Low-temperature Co-fired Ceramics (LTCC) technology has exerted a pivotal part in the production of multilayer ceramic circuits, mainly applied to the medical applications, automotive productions and communication devices [1]. LTCC materials are demanded to have a low sintering temperature (≤ 950 °C) [2–4]. Additionally, the dielectric ceramic, which is mainly used in LTCC, required with high quality factor ($Q\times f$) at a certain dielectric constant (ε_r), and a near-zero temperature coefficient of resonant frequency (τ_f) for stability [5].

As we know, $(Zn_{1-x}Mg_x)TiO_3$ ceramic has a relatively medium dielectric constant and excellent $Q\times f$ value. For instance, Chang et al [6] reported $(Zn_{1-x}Mg_x)TiO_3$ ceramics with the dielectric properties of: ε_r ~ 21, $Q\times f$ ~ 13,600 GHz, and τ_f ~ − 86 ppm °C^{-1} by solid-state reaction at 900 °C. Hsieh et al [7] synthesized 4 wt% Bi_2O_3-doped ZMT ceramic which had microwave dielectric properties of: ε_r ~ 25, $Q\times f$ ~ 70,000 GHz and τ_f ~ − 10 ppm °C^{-1} when sintered at 1000 °C. Our previous work has demonstrated the dielectric properties of $Zn_{0.9}Mg_{0.1}TiO_3$ (ZMT) ceramic with 0.5 wt% ZnO–B_2O_3–SiO_2 (ZBS) glass sintered at 900 °C: ε_r ~ 20.53, $Q\times f$ ~ 61,630 GHz (at 7.44 GHz), τ_f ~ − 76 ppm °C^{-1}. We also found extra TiO_2 could adjust the τ_f value of ZMT from negative to near zero. $Zn_{0.9}Mg_{0.1}TiO_3$ + 3 wt% ZBS + 10 wt% TiO_2 was well sintered at 900 °C and obtained the microwave dielectric properties: ε_r ~ 24.83, $Q\times f$ ~ 44,342 GHz, τ_f ~ 3.44 ppm °C^{-1} [8]. In this work, we try to use another microwave dielectric material to adjust the τ_f of ZMT to zero.

Although the negative temperature coefficient and high sintering temperature of $(Zn_{1-x}Mg_x)TiO_3$ ceramic limit its application, how to excel the dielectric properties of ZMT is deserved studied. Kim et al. [9] investigated the microwave dielectric properties of $(Zn_{1/3}Nb_{2/3})_xTi_{1-x}O_2$ system, which showed a composition of x = 0.5 with high dielectric constant of 95, $Q\times f$ ~ 15,000 GHz and τ_f = + 237 ppm °C^{-1}. Meanwhile, Nenasheva et al. [10] reported that in the $(1-x)ZnNb_2O_6$–$xZn_{0.17}Nb_{0.33}Ti_{0.5}O_2$ system, ceramics with great microwave dielectric properties of ε_r ~ 43.8, $Q\times f$ ~ 35,000 GHz at f = 9 GHz and τ_f ~ 0 ppm °C^{-1} for x = 0.66 at 1080 °C.

Thus, considering a large dielectric constant and positive τ_f values of $(Zn_{1/3}Nb_{2/3})_xTi_{1-x}O_2$ (ZNT), it was chosen

✉ Enzhu Li
lienzhu@uestc.edu.cn

[1] National Engineering Research Center of Electromagnetic Radiation Control Materials, University of Electronic Science and Technology of China, Chengdu 610054, China

[2] Key Laboratory of Multi-Spectral Absorbing Materials and Structures of Ministry of Education, University of Electronic Science and Technology of China, Chengdu 610054, China

to adjust the dielectric properties of ZMT. In addition, the phase composition, microstructure and microwave dielectric properties of ceramics have been investigated systematically.

2 Materials and methods

The ZMT and ZNT ceramics were prepared by a conventional solid-state route. High-purity ZnO (Liuzhou at the Zinc Product Co., Ltd, Liuzhou, China, 99.7%), MgO (Industrial development zone, Mulan Town, Xindu, Chengdu, China, 98.0%), TiO_2 (Xiantao Zhongxing Electronic Materials Co., Ltd, Hubei, China, 99.9%) and Nb_2O_5 (Xiantao Zhongxing Electronic Materials Co., Ltd, Hubei, China, 99.9%) powders were used as the starting materials. The powders were weighed as $Zn_{0.9}Mg_{0.1}TiO_3$ and then ball milled in a nylon jar with zirconia balls for 8 h in the deionized water. The mixtures were dried and calcined at 900 °C for 4 h in air. To prepare sample of ZNT, ZnO, Nb_2O_5 and TiO_2 were mixed according to the formula of $Zn_{0.15}Nb_{0.3}Ti_{0.55}O_2$ for 6 h in the deionized water, then the mixture was dried and calcined at 950 °C for 4 h in air. The obtained ZMT, ZNT and ZBS glass powders [the ZBS glass fabricated by our lab with a molar ratio is (Zn:B:Si) 5:8:1] were weighed as (1 − x)ZMT–xZNT-3 wt% ZBS (x = 0.1–0.2) and re-milled in a nylon jar with zirconia balls for 8 h in the deionized water again, after that, they were dried and added with 3 wt% acrylic acid as binder to form pellets. The last pellets were uniaxially pressed into cylindrical disks (15 mm in diameter and 8 mm in height) under a pressure of 20 MPa. The samples were sintered at the temperature of 900 °C for 4 h with a heating rate of 2 °C min^{-1}.

The crystal structure of ceramics was measured by an X-ray diffractometer (XRD Rigaku Industrial Corporation, Japan) by using Cu kα radiation. The exact structural parameters, such as lattice parameter, cell volume, bond length and bond valence are obtained by GSAS-EXPGUI program [11]. Because of the multiphase coexistence in our samples, the refinement parameters including lattice parameters, profile parameters, background, thermal vibration parameters and weight fractions are refined step-by-step. The validities of the refined results were evaluated by the reliability factor of weighted pattern (R_{wp}), reliability factor of weighted pattern (R_p), and goodness of fit (χ^2). The microstructure was examined of samples using a scanning electron microscopy (SEM, JSN-6490LV, Japan). The bulk densities of the sintered samples were determined by the Archimedes method. Shrinkage of the specimens during heat treatment was measured using a horizontal loading dilatometer with alumina rams and boats (Model DIL402C, Netzsch In-struments, Germany). The relative permittivity ε_r and the unloaded quality factor $Q \times f$ was measured by the Hakki–Coleman dielectric resonator method with an HP83752A network analyzer (HP83752A, the United States). The temperature coefficient of the resonant frequency τ_f value can be obtained by using the following equation:

$$\tau_f = \frac{f_{85} - f_{25}}{f_{25} \times 60} \times 10^6 \ (\text{ppm}/^\circ\text{C}) \quad (1)$$

where f_{85} and f_{25} are the reasonant frequencies at 85 and 25 °C respectively.

3 Results and discussion

The X-ray diffraction patterns of (1 − x)ZMT–xZNT-3 wt% ZBS ceramics sintered at 900 °C for 4 h are given in Fig. 1. As seen, rhombohedral structure of $ZnTiO_3$ (JCPDS # 26-1500) with a group of R-3 (148) and tetragonal structure of $Zn_{0.15}Nb_{0.3}Ti_{0.55}O_2$ (JCPDS # 79-1186) with a space group of *P42/mnm* (136) are the main crystalline phases. Cubic structure of $Zn(BO_2)_2$ (JCPDS # 39-1126) and hexagonal structure of Zn_2SiO_4 (JCPDS #08-0492) are co-existed. The appearance of $Zn(BO_2)_2$ phase and Zn_2SiO_4 phase mainly originates from ZBS glass referring to ZBS phase diagram [12]. And the peak intensities of $Zn_{0.15}Nb_{0.3}Ti_{0.55}O_2$ phase increase along with the increase of its content. However, additional phase of Zn_2TiO_4 (JCPDS # 19-1483) is observed at x = 0.15–0.2.

To further better understanding the structural variation of ZMT and ZNT phases, Rietveld refinement was carried out. Due to the multiphasic systems, the main crystal phases have the greatest impact on the performance of ceramic. It is difficult to conduct the refinement of five phases. Meanwhile, the relative content of Zn_2SiO_4 is very low, thus, we have refined for four phases except Zn_2SiO_4. Generally, in polycrystalline poly phase ceramics, phase content is an important factor to determine the relative density and microwave dielectric properties. The weight fraction of each phase is given in Fig. 2. Obviously, the amount of ZMT decreases, while ZnB_2O_4 varies with no certain regular pattern. ZNT phase contents increase in the whole range. Zn_2TiO_4 phase appeared at x = 0.15, then increase along with x value, further, the largest increase rate of ZNT (35.20%) is observed with x = 0.125–0.150, which is much greater than the formation of Zn_2TiO_4 phase.

Besides, the variations of lattice parameters are shown in Fig. 3a. Lattice parameters and cell volume for ZMT phase all decreased from x = 0.1–0.125 and x = 0.175–0.20. For ZNT phase, declining trend also observed at x = 0.125. To explain this unusual change, the normalized bond length [defined as the ratio of actual bond length to the ideal bond length (sum of effective ionic radii)] [13] of each cation are plotted in Fig. 3b, which can illustrate that the oxygen octahedron is either elongated or compressed. The variations of

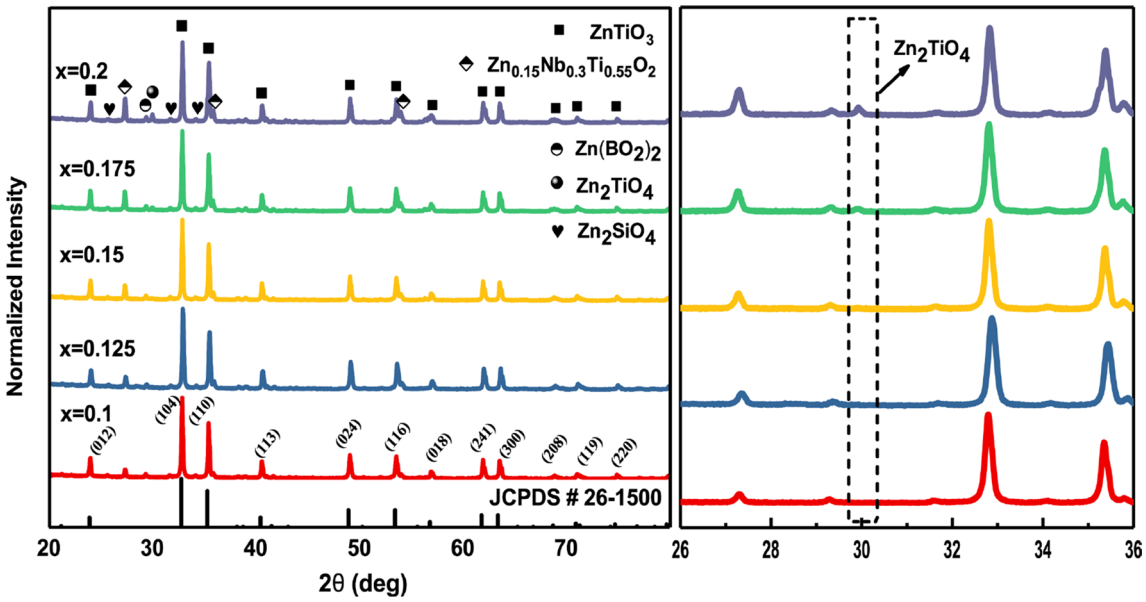

Fig. 1 X-ray diffraction patterns of (1 − x)ZMT–xZNT-3 wt% ZBS ceramics sintered at 900 °C for 4 h

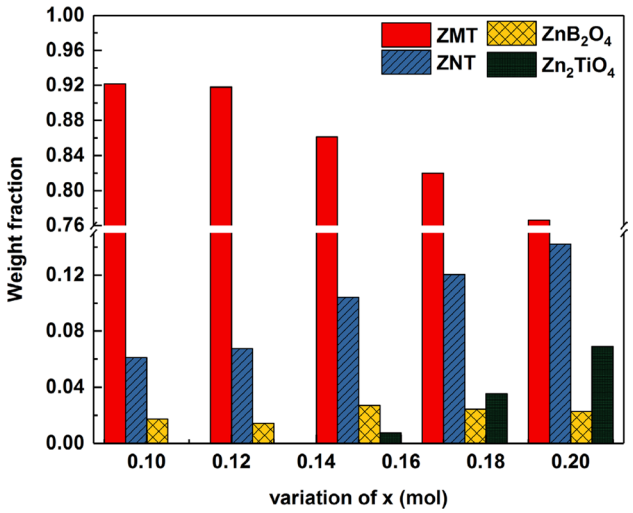

Fig. 2 The weight fraction of each phase after Rietveld refinement

normalized bond length are shown in. For ZMT phase, ionic radii of Zn^{2+} Mg^{2+} and Ti^{4+} (CN = 6) is 0.74, 0.72, 0.605 Å, respectively. For O^{2-} (CN = 3), ionic radius is 1.36 Å.

As defied, Zn–O1(2), Mg–O1(2) and Ti–O1(2) bonds are compressed, while Zn–O1(1), Mg–O1(1) and Ti–O1(1) elongated. It is noting that the normalized bond length of Mg–O1(1) bond varies from 0.961 to 1.3925. Obvious decrease and increase tendencies are observed at x = 0.125–0.175 and 0.175–0.20 in Mg–O1(2). However, more dramatically decrease is obtained for Mg–O1(1) at x = 0.10–0.125 and 0.175–0.20 and increase at x = 0.125–0.175. Subsequently, oxygen octahedron is mainly influenced by the variations of Mg–O1(1) bond, which leads to the same variation for cell volume of ZMT phase.

The exact structural information is listed in Table 1. Calculated pattern is overlaid on the observed pattern and different vertical marks referring to the Bragg positions of $Zn_{0.9}Mg_{0.1}TiO_3$, $Zn_{0.15}Nb_{0.3}Ti_{0.55}O_2$, $Zn(BO_2)_2$ and Zn_2TiO_4 phases are shown in Fig. 4. The differences between the observed and calculated patterns are placed at the bottom. The refined results indicate the reliability of refined data.

The SEM images of (1 − x)ZMT–xZNT-3 wt% ZBS are exhibited in Fig. 5. As seen, the ceramics have a compact structure for each composition. The grain boundary is clearly visible. Grain size has a narrow distribution of 0.12–0.15 μm and increases not significantly.

As mentioned above, the relatively density is important for microwave dielectric properties. The relative densities of (1 − x)ZMT–xZNT-3 wt% ZBS samples sintered at 900 °C for 4 h are shown in Fig. 6. The relative density is calculated through the following equations [14]:

$$\rho_{theo} = \frac{nA}{V_c N_A} \tag{2}$$

$$\rho'_{theo} = \frac{w_1 + w_2 + w_3 + w_4 + w_5}{w_1/\rho_{theo1} + w_2/\rho_{theo2} + w_3/\rho_{\rho theo3} + w_4/\rho_{theo4} + w_5/\rho_{theo5}} \tag{3}$$

$$\rho_{relative} = \frac{\rho_{bulk}}{\rho_{theo}} \tag{4}$$

where n, A, V_c and N_A are the number of atoms in unit cell, atom weight (g mol^{-1}), cell volume and Avogadro number

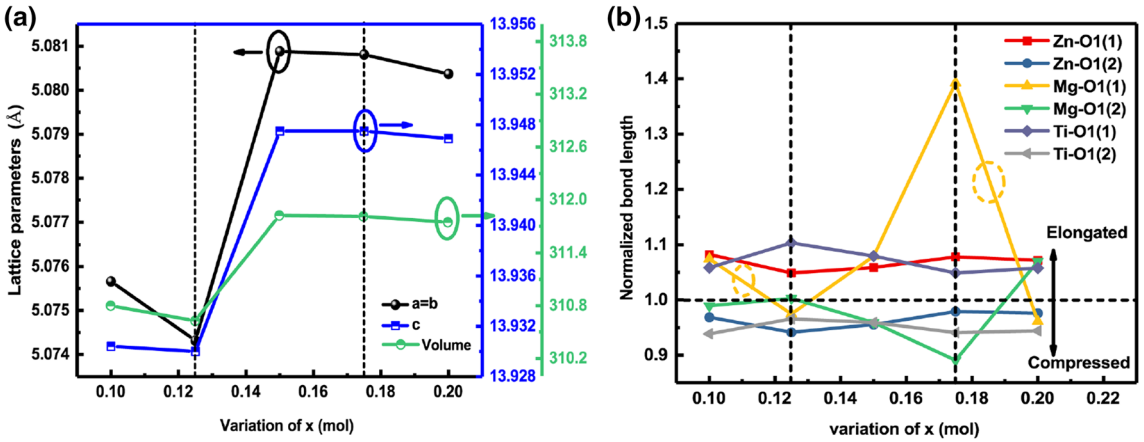

Fig. 3 Rietveld refinement results of ZMT phase for **a** variation of lattice parameters, **b** normalized bond length of Zn/Mg/Ti/–O bond

Table 1 Structural parameters for (1 − x)ZMT–xZNT system after Rietveld refinement

x (mol)	0.1	0.125	0.15	0.175	0.2
ZMT					
a = b (Å)	5.07566 (4)	5.07432 (4)	5.08088 (4)	5.08081 (4)	5.08037 (5)
c (Å)	13.9304 (1)	13.9300 (2)	13.9475 (1)	13.9475 (2)	13.9469 (2)
V(Å^3)	310.800 (4)	310.628 (5)	311.823 (4)	311.812 (5)	311.746 (6)
ZNT					
a = b (Å)	4.6236 (2)	4.6232 (2)	4.6272 (1)	4.6286 (1)	4.6299 (1)
c (Å)	2.9881 (3)	2.9847 (2)	2.9886 (1)	2.9898 (1)	2.9904 (1)
V(Å^3)	63.879 (7)	63.797 (7)	63.991 (4)	64.057 (4)	64.103 (4)
$Zn(BO_2)_2$					
V(Å^3)	414.50 (4)	415.007 (2)	415.462 (3)	417.568 (2)	417.697 (3)
V(Å^3)			299.916 (2)	301.348 (1)	302.142 (3)
W_{f1}	0.92174	0.91809	0.86113	0.81995	0.76613
W_{f2}	0.06108	0.06759	0.10431	0.12042	0.14205
W_{f3}	0.01718	0.01431	0.02705	0.02434	0.02273
W_{f4}	0	0	0.00751	0.03529	0.06910
R_{wp} (%)	8.09	8.20	8.23	8.00	8.47
R_p (%)	5.87	6.00	6.00	6.00	6.51
χ^2	1.95	1.85	1.94	1.88	2.08

V volume of unit cell, W_{f1} weight fraction of $Zn_{0.9}Mg_{0.1}TiO_3$, W_{f2} weight fraction of $Zn_{0.15}Nb_{0.3}Ti_{0.55}O_2$, W_{f3} weight fraction of $Zn(BO_2)_2$, W_{f4} weight fraction of Zn_2TiO_4, R_{wp} reliability factor of weighted pattern, R_p reliability factor of weighted pattern, χ^2 goodness of fit

(mol^{-1}) [15]. 1–5 represent for ZMT, ZNT, $Zn(BO_2)_2$, Zn_2TiO_4 phases and ZBS glass. For ZMT and $Zn(BO_2)_2$, $n = 6$. For ZNT, $n = 2$. For Zn_2TiO_4, $n = 4$. The density of ZBS glass is adopted as 3.57 g cm^{-3}. The calculated results are listed in Table 2.

According to Eq. 2, relative density should have an opposite tendency with cell volume. For ZMT phase, the theoretical density increases at x = 0.1–0.125 and 0.175–0.2 and decreases at 0.125–0.175. For ZNT, $Zn(BO_2)_2$ and Zn_2TiO_4 phases, these changes also show the opposite tendency with cell volume. Therefore, the variation of whole theoretical density should be attributed to the change of volume fraction of each phase. The relatively of the sintered ceramics obtains a largest value of 95.38% at x = 0.175, meaning a most compact structure was formed.

The dielectric constant is shown in Fig. 5. In polyphase ceramics, the densification and second phase contents are the main reasons determining the ε_r value. Due to all the ceramics have a relative density larger than 93%, thus, we mainly consider the influences from the second phase contents.

There are many classical mixture rules for predicting the ε_r value, such as the Parallel mixing rule, Serial mixing model, Lichtenecker logarithmic mixing rule and Maxwell–Garnett rule, et al. Thus, we choose some of the models

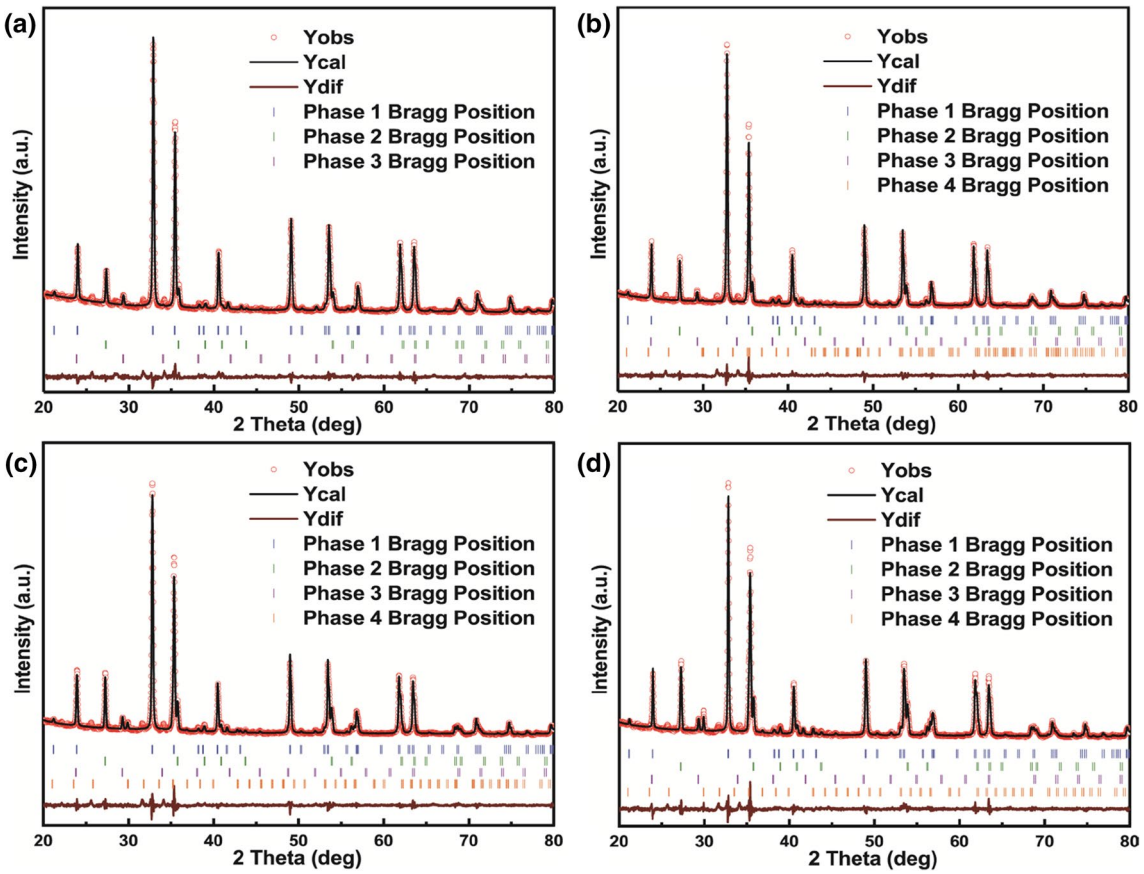

Fig. 4 XRD pattern of (1 − x)ZMT–xZNT-3 wt% ZBS ceramic sintered at 900 °C for 4 h after refinement: **a** x = 0.125, **b** x = 0.15, **c** x = 0.175, **d** x = 0.2

to predict the variation of our experiments. The equations used are as follows [16, 17].

$$\begin{aligned} &\ln \varepsilon_{eff} = V_1 \ln \varepsilon_1 + V_2 \ln \varepsilon_2 + V_3 \ln \varepsilon_3 + V_4 \ln \varepsilon_4 + V_5 \ln \varepsilon_5 \quad \text{(Logarithmic mixing model)} \\ &\varepsilon = V_1\varepsilon_1 + V_2\varepsilon_2 + V_3\varepsilon_3 + V_4\varepsilon_4 \quad \text{(Parallel mixing model)} \\ &\varepsilon^{-1} = V_1{\varepsilon_1}^{-1} + V_2{\varepsilon_2}^{-1} + V_3{\varepsilon_3}^{-1} + V_4{\varepsilon_4}^{-1} \quad \text{(Serial mixing model)} \end{aligned} \tag{5}$$

Besides, the ε_r value should be corrected with porosity using the following equation:

$$\varepsilon_r = \varepsilon_{rc}\left(1 - \frac{3p(\varepsilon_{rc} - 1)}{2\varepsilon_{rc} + 1}\right) \tag{6}$$

The dielectric constant of each part is obtained from the literatures. For ZMT phase, $\varepsilon_r = 23$, for ZNT phase, $\varepsilon_r = 94$, for Zn_2TiO_4 phase, $\varepsilon_r = 21$, for ZBS glass, $\varepsilon_r = 6.5310$. And the ε_r for ZnB_2O_4 is calculated by Clausius–Mosotti equation by using the ionic polarizability. The volume fractions and dielectric constant of each part are given in Table 3.

The comparisons are shown in Fig. 6. The variations of the experimental results are similar with the theoretical models, which also illustrates the second phase contents are vital in the ceramics. Besides, the parallel mixing model show the best predictability.

The variation of $Q \times f$ value is shown in Fig. 7a. The $Q \times f$ values are affected by many aspects, such as relative density, grain size and second phase contents. The compositions all have a relative density higher than 94% (except x = 0.125), so, relative density is not the primary factors. Besides, grain size distributions have a similar value of (0.12–0.15 μm). Thus, we infer the second phase contents dominate the dielectric loss due to a smaller $Q \times f$ value of ZNT ($Q \times f = 10{,}000$ GHz), Zn_2TiO_4 ($Q \times f = 20{,}000$ GHz) and ZBS glass ($Q \times f = 4465$ GHz) [18].

The variations of τ_f values are shown in Fig. 7b. It is clear that the τ_f values change from negative to positive with the variation of x. The τ_f values change from negative to positive with the variation of x. When x = 0.175, the value of τ_f is near to zero ($\tau_f = -3.46$ ppm °C^{-1}), which matches well with

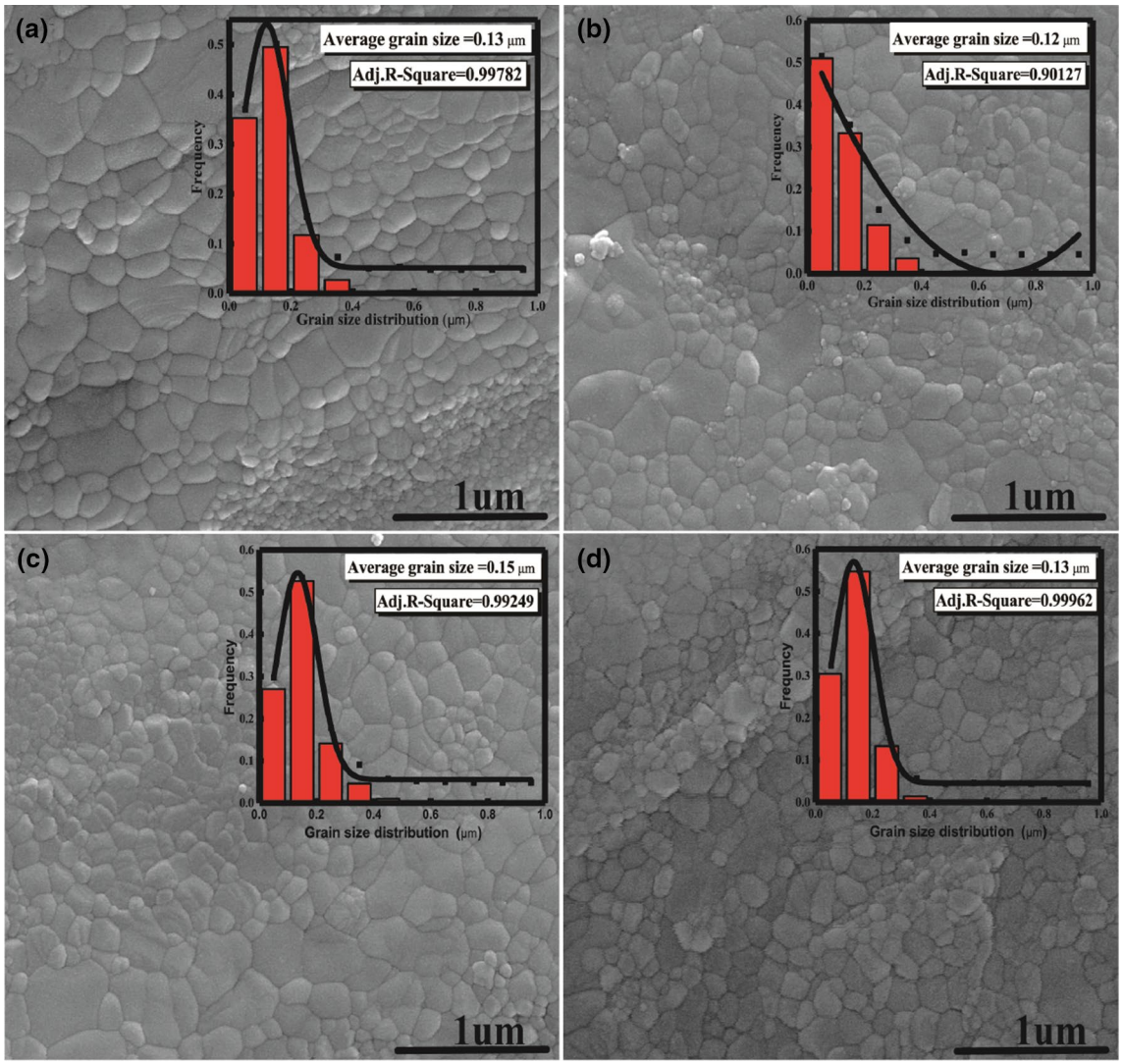

Fig. 5 SEM micrographs and grain size distribution of (1 − x)ZMT–xZNT-3 wt% ZBS ceramics where **a**–**d** stand for x = 0.1, 0.125, 0.15 and 0.2

our calculation by the formula (7) [19] (theoretical value of x = 0.21 when $\tau_f = 0$). Definitely, ZNT phase makes great improvements to the τ_f value of ZMT (the τ_f of ZMT and ZNT is − 70 and 323 ppm °C^{-1}, respectively [20]).

$$\begin{aligned} \tau_f &= V_1\tau_{f1} + V_1\tau_{f1} \\ 1 &= V_1 + V_2 \end{aligned} \tag{7}$$

Similarly, τ_f value is also affected by the intrinsic factor. For the intrinsic part, τ_f value is influenced by the bond strength and distortion of oxygen octahedron. A larger oxygen octahedron distortion means a lower vibration restoring force, which presents a lower $|\tau_f|$ value [21]. Corresponding to the normalized bond lengths, MgO_6 octahedrons have the largest contributions to the cell volume. Thus, we mainly discuss the variation of Mg–O bond strength and their distortions. The bond strength s_{ij}, bond valence v_{ij} and distortion of octahedron Δ can be calculated using the Eqs. (8–11) [22].

$$v_{ij} = \exp\left(\frac{R_{ij} - d_{ij}}{b}\right) \tag{8}$$

$$s = \left(\frac{R}{R_1}\right)^{-N_1} \tag{9}$$

$$V_i = \sum v_{ij} \tag{10}$$

$$\Delta = \frac{d_{l\arg est(i-o)} - d_{smallest(i-o)}}{d_{average(i-o)}} \tag{11}$$

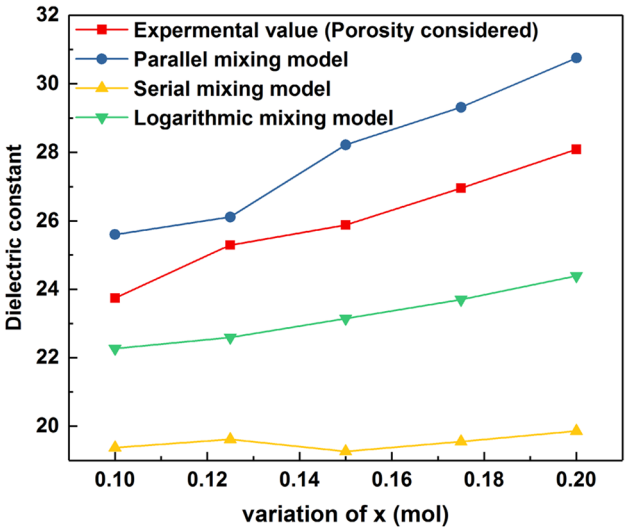

Fig. 6 Comparisons between the experimental ε_r values and theoretical values of (1 − x)ZMT–xZNT-3 wt% ZBS ceramic

where R_{ij} is Mg–O bond valence parameter from the previous report with a value of 1.693; b is commonly taken as 0.37 Å; R_1, N_1 are taken as 1.622, 4.290, respectively. The calculations are listed in Table 4.

According to the equation, bond strength has an opposite trend with cell volume. The larger cell volume refers to a larger bond length, which determines a lower combination between cation and oxygen and a lower the bond strength. For the distortion of MgO_6 oxygen octahedron, if the τ_f value is closer to zero, the distortion will be larger, which is consistent with the variation of distortion and the largest value obtained at x = 0.175. And it is well known that the τ_f is related to the thermal expansion coefficient (α_L) and the variation of dielectric constants with temperature (τ_ε). It could be described as the following Eq. (12) [23]:

$$\tau_f = -\left(\alpha_L + \frac{1}{2}\tau_\varepsilon\right) \tag{12}$$

Nearly all the ceramics, the α_L is generally equal to 10 ppm °C^{-1}. So, the τ_ε plays a vital role with τ_f. The τ_ε value can be derived as the macroscopic Clausius–Mossotti equation when the pressure is constant:

$$\tau_\varepsilon = \frac{1}{\varepsilon}\left(\frac{\partial \varepsilon}{\partial T}\right) \tag{13}$$

Thus, the variation of τ_f and dielectric constant is consistent.

4 Conclusion

In our work, the influences of rutile $Zn_{0.15}Nb_{0.3}Ti_{0.55}O_2$ phase on the phase composition, microstructure and microwave dielectric properties of $Zn_{0.9}Mg_{0.1}TiO_3$ have been studied in detail. Rietveld refinement results show the coexistence of $Zn_{0.9}Mg_{0.1}TiO_3$, $Zn_{0.15}Nb_{0.3}Ti_{0.55}O_2$, $Zn(BO_2)_2$ and Zn_2TiO_4 phases with certain weight fraction. In $Zn_{0.9}Mg_{0.1}TiO_3$ rhombohedral structure, the variation of Mg–O1 (1) bond is the main reason affecting the cell volume. With ZBS glass added, the dense ceramics sintered (> 95%) at x = 0.175 at 900 °C with a smaller grain size of 0.12 μm. In this ceramic, second phase contents determine the variations of dielectric constant and $Q \times f$ value. The τ_f influences by the distortion of MgO_6 oxygen octahedron except the second phase content as

Table 2 Theoretical density and relative density of (1 − x)ZMT–xZNT-3 wt% ZBS ceramic

x (mol)	ρ_{theo1}	ρ_{theo2}	ρ_{theo3}	ρ_{theo4}	ρ_{theo}	ρ_{bulk}	$\rho_{relative}$ (%)
0.1	5.0377	4.9912	3.6299		4.9078	4.626	94.26
0.125	5.0405	4.9976	3.6254		4.9152	4.572	93.02
0.15	5.0212	4.9825	3.6215	5.3743	4.8768	4.594	94.20
0.175	5.0214	4.9773	3.6032	5.3488	4.8873	4.662	95.38
0.2	5.0224	4.9738	3.6021	5.3347	4.8981	4.613	94.18

Table 3 Volume fractions and ε_r values of (1 − x)ZMT–xZNT-3 wt% ZBS ceramic

x (mol)	V_{f1}	V_{f2}	V_{f3}	V_{f4}	V_{f5}	Measured ε_r	ε_r (porosity consider)
0.1	0.8552	0.0572	0.0221	0	0.0655	22.76	23.74
0.125	0.8526	0.0635	0.0185	0	0.0656	23.72	25.29
0.15	0.7965	0.0972	0.0347	0.0065	0.065	24.69	25.88
0.175	0.7600	0.1126	0.0314	0.0307	0.0652	26.14	26.95
0.2	0.7116	0.1332	0.0294	0.0604	0.0653	26.7	28.09

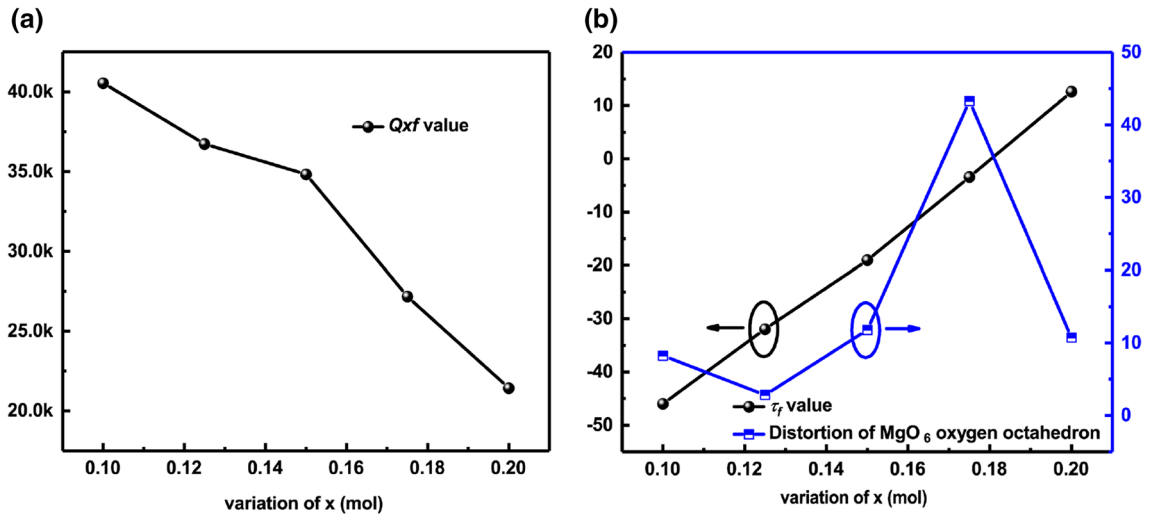

Fig. 7 The $Q \times f$ and τ_f values of (1 − x)ZMT–xZNT-3 wt% ZBS ceramic sintered at 900 °C

Table 4 Bond length, bond strength, bond valence of Mg–O, and distortion of MgO_6 oxygen octahedron of (1 − x) ZMT–xZNT-3 wt% ZBS ceramic sintered at 900 °C

x (mol)	d_{Mg-O}	s_{Mg-O}	S_{Mg-O}	v_{Mg-O}	V_{Mg-O}	Δ (%)	τ_f (ppm °C^{-1})
0.1	2.235 × 3	0.253 × 3	1.839	0.231 × 3	1.813	8.23	− 45.95
	2.058 × 3	0.360 × 3		0.373 × 3			
0.125	2.027 × 3	0.384 × 3	2.171	0.405 × 3	2.252	2.85	− 31.93
	2.086 × 3	0.340 × 3		0.346 × 3			
0.15	2.245 × 3	0.248 × 3	1.979	0.225 × 3	2.002	11.80	− 19.03
	1.995 × 3	0.412 × 3		0.442 × 3			
0.175	2.876 × 3	0.086 × 3	1.954	0.041 × 3	2.072	43.28	− 3.46
	1.852 × 3	0.566 × 3		0.650 × 3			
0.2	1.998 × 3	0.409 × 3	1.999	0.438 × 3	2.027	10.74	12.57
	2.225 × 3	0.258 × 3		0.237 × 3			

d_{Mg-O} bond length of Mg–O, R_{Mg-O} bond valence parameter of Mg_O, s_{Mg-O} *and* S_{Mg-O} bond strength of Mg–O and sum of all of the Mg–O bond strengths, v_{Mg-O} *and* V_{Mg-O} bond valence of Mg–O and sum of all of the Mg–O bond valences, Δ distortion of MgO_6 oxygen octahedron

well. The ceramics posses the best combination properties at 900 °C with a microwave dielectric property: $\varepsilon_r = 26.14$, $Q \times f = 27{,}184$ GHz, $\tau_f = -3.46$ ppm °C^{-1}.

Acknowledgements This work is partly supported by Science and Technology Planning Project of Guangdong Province, China (No. 2017A010103001).

References

1. D. Zhou, J. Li, L.-X. Pang, D.-W. Wang, I.M. Reaney, J. Mater. Chem. C **5**, 6086–6091 (2017)
2. M.T. Sebastian, H. Jantunen, Int. Mater. Rev. **53**, 57–90 (2013)
3. Y. Chen, E. Li, S. Duan, S. Zhang, ACS Sustain. Chem. Eng. **5**, 10606–10613 (2017)
4. Y. Chen, E. Li, M. Zou, H. He, S. Zhang, J. Mater. Sci. Mater. Electron. **28**, 13132–13138 (2017)
5. J. Guo, D. Zhou, L. Wang, H. Wang, T. Shao, Z.M. Qi, X. Yao, Dalton Trans. **42**, 1483–1491 (2013)
6. Y.-S. Chang, Y.-H. Chang, I.-G. Chen, G.-J. Chen, Solid State Commun. **128**, 203–208 (2003)
7. M.-L. Hsieh, L.-S. Chen, S.-M. Wang, C.-H. Sun, M.-H. Weng, M.-P. Houng, S.-L. Fu, Japn. J. Appl. Phys. **44**, 5045–5048 (2005)
8. E. Li, P. Zhang, S. Duan, J. Wang, Y. Yuan, B. Tang, J. Alloys Compds. **647**, 866–872 (2015)
9. E.S. Kim, B.S. Chun, R. Freer, R.J. Cernik, J. Eur. Ceram. Soc. **30**, 1731–1736 (2010)
10. E.A. Nenasheva, S.S. Redozubov, N.F. Kartenko, I.M. Gaidamaka, J. Eur. Ceram. Soc. **31**, 1097–1102 (2011)
11. B.H. Toby, J. Appl. Crystallogr. **34**, 210–213 (2001)
12. M.A. Eldem, B.R. Orton, A. Whitaker, J. Mater. Sci. **22**, 4139–4143 (1987)
13. M.M. Mao, X.Q. Liu, X.M. Chen, J. Am. Ceram. Soc. **94**, 2506–2511 (2011)
14. T. Takahiro, S.F. Wang, Y. Shoko, J. Sei-Joo, R.E. Newnham, J. Am. Ceram. Soc. **77**, 1909–1916 (1994)
15. H. Yang, E. Li, S. Duan, H. He, S. Zhang, Mater. Chem. Phys. **199**, 43–53 (2017)

16. D.-W. Kim, H.B. Hong, K.S. Hong, Japn. J. Appl. Phys. **41**, 1465–1469 (2002)
17. J. Guo, S.S. Berbano, H. Guo, A.L. Baker, M.T. Lanagan, C.A. Randall, Adv. Func. Mater. **26**, 7115–7121 (2016)
18. H. Jeong, C. Huh, T.-Y. Lim, J.-H. Kim, M. Lee, D.-W. Jeon, J. Hwang et al., J. Non-Cryst. Solids **423–424**, 25–29 (2015)
19. D. Kim, D. Kim, K.S. Hong, J. Mater. Res. **15**, 1331–1335 (2000)
20. Y.-C. Lee, W.-H. Lee, F.-T. Shiao, Japn. J. Appl. Phys. **43**, 7596–7599 (2004)
21. I.D. Brown, D. Altermatt, Acta Crystallogr. A **41**, 244–247 (2010)
22. I.D. Brown, R.D. Shannon, Acta Crystallogr. Sect. A **29**, 266–282 (2010)
23. D. Zhou, L.-X. Pang, D.-W. Wang, C. Li, B.-B. Jin, I.M. Reaney, J. Mater. Chem. C **5**, 10094–10098 (2017)